Combustion and Flame 228 (2021) 210–217

Contents lists available at ScienceDirect

Combustion and Flame

journal homepage: www.elsevier.com/locate/combustflame

Tuning the reactivity and energy release rate of I_2O_5 based ternary thermite systems

Feiyu Xu[a,b], Prithwish Biswas[a], Giorgio Nava[a], Joseph Schwan[a], Dylan J. Kline[a,b], Miles C. Rehwoldt[a,b], Lorenzo Mangolini[a], Michael R. Zachariah[a,*]

[a] University of California, Riverside, CA 92521, United States
[b] University of Maryland, College Park, MD 20742, United States

ARTICLE INFO

Article history:
Received 8 January 2020
Revised 27 December 2020
Accepted 29 December 2020

Keywords:
Nanothermite
Biocidal
Iodine pentoxide
Energy release rate

ABSTRACT

Iodine pentoxide (I_2O_5) based nanothermites are one of the most promising candidates for biocidal energetic materials due to superior reactivity and high iodine content. However, the tunability of nanothermites, which is important for biocidal performance, has not been fully exploited for I_2O_5 based nanothermites. In this work, I_2O_5 with various fuels (Al, Ti, Si) and their mixtures (i.e., a ternary system) have been investigated. The reactivity and flame temperature were evaluated by a pressure cell coupled with a spectrometer. Temperature-Jump time-of-flight mass spectrometry (T-Jump TOFMS) was used to probe the reaction mechanism and iodine release behavior, along with a high-speed camera to capture the ignition event. I_2O_5 showed distinct reactivity with different fuels. As a result, by varying the fuel composition of ternary systems, the combustion properties can be tuned. Rapid heating experiments revealed that the reaction initiation was shifted from gas phase dominated to condensed phase dominated mechanism after introducing Ti or Si into Al/I_2O_5 system. Further analysis of the ternary systems found that the energy release rate correlates with burn time instead of flame temperature. This study shows an approach to tune the reactivity and energy release rate of I_2O_5 based nanothermites without compromising the energy density.

1. Introduction

Energetic materials with biocidal components have been developed as a method to neutralize potential threat of biological warfare agents [1]. The combination of a thermal pulse and remnant biocidal agents have been shown to be highly efficient in killing spores, bacteria, etc. [2–3]. Nanothermites are a novel class of energetic materials that consists of near-homogenous mixtures of nano-sized fuel and oxidizer particles, and offer in many cases a higher energy density and flame temperature than traditional monomolecular systems [4–5]. A variety of biocidal agents have been incorporated in nanothermite systems, such as silver-containing oxides [6–7], persulfate salt [8], metal iodates [9] and iodine pentoxide (I_2O_5) [10–11]. I_2O_5 has received considerable attention because it is a highly aggressive oxidizer in its own right, but also has a high iodine content, and has been shown to be effective in spore inactivation [12].

One of the advantages of nanothermites is their potential tunability, certainly relative to traditional mono-molecular energetics. The reactivity of nanothermites can be tuned over a wide range, by varying stoichiometry, size and microstructure [13–15]. Additives have also been used but usually at the expense of energy density [16]. For biocidal applications, the energy release rate is also important because it is related to the thermal output profile and timescale of biocides release, which can affect the biocidal performance [3]. Therefore, an ideal biocidal energetic system should have tunable reactivity and energy release rate without compromising energy density. Although aluminum is acknowledged as the most important practical fuel, titanium and silicon are also important candidate fuels using metrics of gravimetric and volumetric oxidation heats [17], and have previously been seen to be reactive in this context [18–19]. This leads to a conjecture that combining different fuels may offer the opportunity to simultaneously maintain high energy density and have a tunable energy release rate.

Herein, the combustion performance of Al, Ti and Si with I_2O_5 was investigated. Based on these results, as will be discussed, ternary Al/Ti/I_2O_5 and Al/Si/I_2O_5 systems were also investigated because of the distinct timescale of individual reactions in the sys-

* Corresponding author.
E-mail address: mrz@engr.ucr.edu (M.R. Zachariah).

https://doi.org/10.1016/j.combustflame.2020.12.047
0010-2180/

tems. The reactivity and flame temperature were measured by a pressure cell equipped with a spectrometer. The ignition behavior was studied by Temperature-Jump (T-Jump) wire ignition coupled with high speed imaging. The reaction mechanism was probed by a time resolved linear time-of-flight mass spectrometry (TOFMS). These results provide insights into how additives and stoichiometry affect the reactivity and energy release rate of ternary thermite systems.

2. Experimental section

2.1. Materials

Aluminum nanopowders (~80 nm, 81 wt% active) were purchased from Novacentrix. Titanium nanopowders (50–80 nm, 70 wt% active) were purchased from US Research Nanomaterials, Inc. Both Al and Ti nanopowders were used as received.

Crystalline silicon nanoparticles were synthesized with a non-thermal plasma reactor. Non-thermal plasma discharges have recently emerged as flexible tools for the synthesis of high-purity inorganic nanomaterials [20–24]. The production approach is scalable and enables a degree of control of the synthesized material properties, most notably crystallinity and particle size, that is currently not within reach of more conventional methods [25–27]. The system used in these experiments comprises a 2'' quartz tube and copper ring electrode connected to a radiofrequency power supply. 700 sccm of an Argon-Silane mixture (1.36% SiH_4 in Ar) are flown in the rector while the pressure is kept at 3 Torr. During the particle synthesis, the plasma power is kept at 160 W. The particle size is around 9 ± 4 nm, where particle size distribution is determined via TEM analysis (Figure S1) from the measurement of a statistical ensemble of 500 particles. TGA results show the active content of this Si is 65%.

Commercial I_2O_5 was purchased from Sigma Aldrich. Prior to use, commercial I_2O_5 was dried at 300 °C for 2 h. Then, the dried samples were ball milled for 2 h in hexane followed by air drying. The as-prepared samples were characterized by XRD (PANalytical EMPYREAN, Cu-Kα source ($\lambda = 1.543$ Å)) and SEM (Nova NanoSEM 450). The size distribution was obtained using Nano Measurer 1.2.

2.2. Pressure cell and temperature measurements

Samples were thoroughly mixed by sonication in hexane and after dried, 25 mg of loose powder was tested in a constant volume combustion cell (~20 cm^3). The measurements were conducted in air and the initial pressure in the combustion cell is 1 atm. The samples were ignited by a nichrome wire upon the application of a DC voltage. Pressure and optical signals were recorded by an oscilloscope. The temporal pressure was obtained with a high frequency pressure transducer (PCB Piezoelectronics). The optical emission was focused by a convex lens and transferred to a photomultiplier tube (Hamamatsu) through a fiber optic cable. Pressurization rate was computed as the peak pressure divided by pressure rise time, i.e., the slope of the pressure rise profile. Burn time was defined as the full width at half maximum (FWHM) of the optical emission. For temperature measurement, the emitted light was dispersed by a spectrometer (Acton SP 500i) coupled with a 32 channel PMT module (Hamamatsu, H7260) and recorded by a high-speed data acquisition (DAQ) system (Vertilon IQSP580). The spectral data was fitted according to Wein's Law using gray body assumption to obtain time-resolved temperature profile. More information regarding temperature measurement is detailed elsewhere [28].

2.3. Temperature-jump (T-Jump) ignition

The ignition behavior of the samples was characterized by T-jump coupled with a high-speed camera (Vision Research Phantom V12.1). Samples were dispersed in hexane by sonication for 30 min. The dispersion obtained after sonication was uniformly coated on the center part of a platinum wire (~1 cm, $d = 76$ µm, OMEGA Engineering Inc.) soldered to the copper leads of the sample holder, with a micro-pipette. Then, the sample holder was inserted into a six-way cross followed by evacuation using a vacuum pump. To ignite the sample, a pulsed square wave signal (~3 ms) was applied to resistively heat the platinum wire. The current across the wire was measured by a Teledyne LeCroy CP030A 30A 50 MHz current probe and the voltage was recorded by a Lecroy LT344 digital oscilloscope. The Callender-Van Dusen equations were used to calculate the temperature of the wire from I-V profile, which showed that wire was heated at a heating rate of ~10^5 K/s to ~1400 K. The ignition process was simultaneously recorded with the synchronized high-speed camera at 67,000 fps through an observation window. The ignition temperature was determined by correlating the optical emission to the wire temperature.

2.4. T-Jump linear time-of-flight mass spectrometry (TOFMS)

T-Jump TOFMS was used to gain insights into the reaction mechanism under rapid heating. The details of the T-Jump TOFMS setup is described elsewhere [29–30]. The sample preparation and rapid heating process are the same as described above in the T-jump ignition section. The prepared sample holder was loaded into the TOFMS chamber (~10^{-6} Torr). Upon rapid heating, the time resolved mass spectra of the reaction products were collected. The evolved reaction products are ionized and accelerated towards the detector and the raw signal is collected by a Teledyne LeCroy 600 MHz oscilloscope.

3. Results and discussion

3.1. Characterization of I_2O_5

I_2O_5 used in this study was prepared by drying and ball milling commercial I_2O_5. It is known that I_2O_5 is hygroscopic and slowly converts to HI_3O_8, and subsequently to HIO_3 under ambient environment [31]. Therefore, as-received commercial I_2O_5 was characterized by XRD to identify its composition. The results (Fig. 1a) showed that the major phase is HI_3O_8 instead of I_2O_5, same as reported in other works [32–33]. To obtain pure I_2O_5, additional dehydration processing was required. In situ heating XRD results showed that the transition from HI_3O_8 to I_2O_5 occurred at around 250–300 °C and I_2O_5 started to decompose at ~360 °C [34]. Accordingly, to remove crystal water and avoid decomposition, commercial I_2O_5 was dried in a furnace at 300 °C for 2 h. In addition, the dried I_2O_5 was ball milled for 2 h to reduce particle size. XRD patterns of different I_2O_5 samples in Fig. 1a show that when commercial I_2O_5 was dried at 250 °C, HI_3O_8 phase disappeared but I_2O_5 phase was not completely formed. When dried at 300 °C, phase pure I_2O_5 with good crystallinity was formed and therefore 300 °C was used for the dehydration of commercial I_2O_5. SEM image of the as-prepared I_2O_5 is shown in Fig. 1b and the size distribution is shown in Figure S2. The particle size ranges from ~0.2 to 4 µm with an average of ~1 µm.

3.2. Single fuel studies: Al/I_2O_5, Ti/I_2O_5 and Si/I_2O_5

Prior to the study of dual fuel systems, I_2O_5 with individual fuels was studied. The theoretical reaction enthalpy per mole

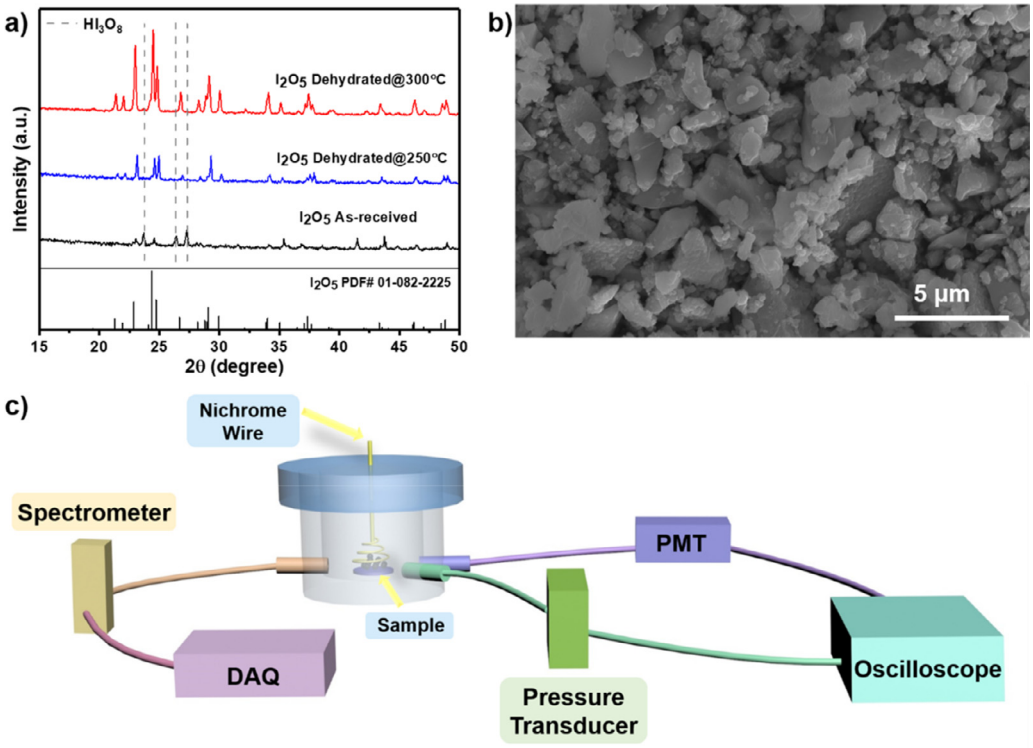

Fig. 1. (a) XRD patterns of the standard (PDF# 01–082–2225), commercial I_2O_5 and I_2O_5 dried at 250 °C and 300 °C (after ball milling). The characteristic peaks of HI_3O_8 (PDF# 01–074–0332) is also shown as dashed lines for comparison. (b) SEM of as-prepared I_2O_5. The size of the particles ranges from 0.2 to 4 μm. (c) Schematic illustration of the pressure cell coupled with a photomultiplier tube, a pressure transducer and a spectrometer for conversion of optical signal, pressure signal and dispersion of emitted light, respectively. The pressure and optical signals were recorded by an oscilloscope to evaluate the reactivity. The spectral data was collected by a high-speed data acquisition (DAQ) system and further processed to obtain flame temperature . (For interpretation of the references to colour in this figure legend, the reader is referred to the web version of this article.)

Table 1
Thermochemistry of reactions between I_2O_5 and various fuels.

Reaction	$-\Delta H^{\circ}_{cal}$ (kJ/mol I_2O_5)	$-\Delta H^{\circ}_{cal}$ (kJ/g)	T_{ad} (K)
$10Al+3I_2O_5 \rightarrow 3I_2+5Al_2O_3$	2247	5.3	4156
$5Ti+2I_2O_5 \rightarrow 2I_2+5TiO_2$	2026	4.5	3924
$5Si+2I_2O_5 \rightarrow 2I_2+5SiO_2$	1856	4.6	3202

I_2O_5 and per mass were calculated along with the isochoric adiabatic flame temperature calculated by CHEETAH code. As shown in Table 1, Al/I_2O_5 not surprisingly has the highest energy density, while Ti/I_2O_5 and Si/I_2O_5 are ~ 15% lower. Adiabatic flame temperature, follows the enthalpy of reaction, shows Al>Ti>Si. Although Al seems to be thermodynamically more favorable, there are kinetic constraints as well that will be explored in this work.

The reactivity of I_2O_5 with three fuels was evaluated in a constant volume combustion cell. As illustrated in Fig. 1c, the combustion cell is equipped with three ports from which signals are collected simultaneously. The pressure and optical signals are converted by a pressure transducer and a photomultiplier tube (PMT), respectively, and are recorded by an oscilloscope for analysis. The third port is interfaced with a spectrometer that converts emitted light into spectral data, which is subsequently collected by a data acquisition (DAQ) system to obtain flame temperature [28]. Interestingly, despite the clear advantage Al has in the thermochemistry (Table 1), the results of pressure cell tests summarized in Table 2, show that Al burns the slowest with smallest peak pressure and pressurization rate. The peak pressure for Ti and Si are 5x and 2x that of Al, respectively. Even more dramatic is the difference in pressurization rate, where Ti is 260 and Si is 43 times higher. This is consistent with the considerably shorter burn times for both Ti and Si relative to Al.

The results suggest that given the much shorter burn time of Ti and Si, one might reasonably consider how mixing these fuels with Al would impact the combustion and energy release profile. Therefore, $Al/Ti/I_2O_5$ and $Al/Si/I_2O_5$ ternary systems will be explored in the remainder of this work.

3.3. I_2O_5 with dual fuels: $Al/Ti/I_2O_5$ and $Al/Si/I_2O_5$

3.3.1. Reactivity and flame temperature

$Al/Ti/I_2O_5$ and $Al/Si/I_2O_5$ ternary mixtures were prepared by varying the weight percentage of Ti or Si in the fuel, from 0 to 100% at an increment of 20%. The total mass of the mixture was held constant. CHEETAH thermochemical code was used to calculate pressure and adiabatic flame temperature for both systems at constant volume condition. The complete results of CHEETAH calculation are shown in Table S1 and S2. As shown in Fig. 2, the peak pressure and pressurization rate both increase with the incremental addition of Ti. Ti/I_2O_5 has the best reactivity: the peak pressure becomes six times higher and the pressurization rate increases by two orders of magnitude. The burn time decreases dramatically with the addition of 20% Ti, but further addition of Ti has limited effect on the burn time. The burn time of Ti/I_2O_5 (~0.1 ms) drops to only one tenth of Al/I_2O_5 (~1.1 ms). These results indicate that given the disparity in reactivity between Ti and Al, this mixture can be used to tune burn properties. The calculated values of peak pressure are higher than experimental results for Al/I_2O_5 only. After adding Ti, the experimental results become significantly higher than calculation results at that are at thermodynamic equilibrium condition. This indicates that Ti/I_2O_5 reaction is likely to be kinetically controlled. The measured flame temperature and calculated adiabatic flame temperature actually show opposite trends.

Table 2
Peak pressure, pressurization rate and burn time of I_2O_5 with various fuels.

Reaction	Peak Pressure (kPa)	Pressurization rate (kPa/ms)	Burn time (ms)
$10Al+3I_2O_5 \rightarrow 3I_2+5Al_2O_3$	260	266	1.1
$5Ti+2I_2O_5 \rightarrow 2I_2+5TiO_2$	1386	69,300	0.1
$5Si+2I_2O_5 \rightarrow 2I_2+5SiO_2$	514	11,540	0.1

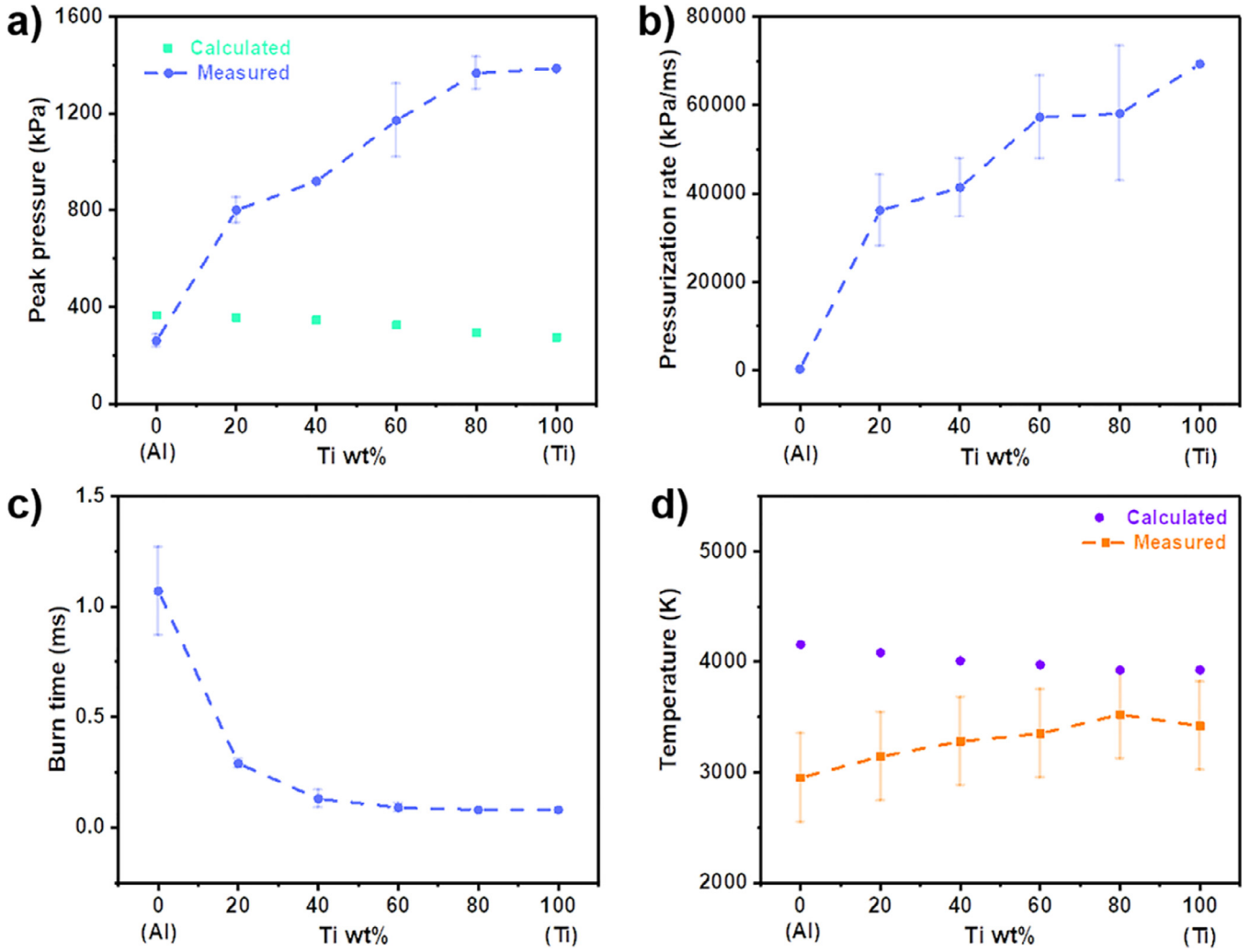

Fig. 2. Experimental and calculated peak pressure (a), pressurization rate (b) and burn time (c) of Al/Ti/I_2O_5 system with different Ti content in fuel. Reactivity increases with increasing Ti content. (d) Adiabatic flame temperature calculated using CHEETAH code and measured flame temperature in pressure cell. The result suggests that Ti/I_2O_5 reaction has higher extent of completion relative to Al/I_2O_5 due to facile kinetics . (For interpretation of the references to colour in this figure legend, the reader is referred to the web version of this article.)

The measured temperature increases with increasing Ti content ranging from ~2900 K to ~3500 K. As expected, the measured temperatures are all lower than the calculated temperatures due to incomplete reaction, but the difference between measured and theory decreases with increased Ti content. This result implies that the Al reaction does not approach completion relative to the Ti reaction [35], and is consistent with the fact while the thermochemistry favors Al, the pressure cell results presented in Table 2 clearly indicate the kinetics of the Ti reaction is much more facile.

If we now consider the Al/Si/I_2O_5 system results shown in Fig. 3, the peak pressure increases with the addition of up to 40% Si to a value 3.4x that of Al/I_2O_5. The pressurization rate also increases upon addition of Si, and peaks at 80% Si content. The burn time decreases dramatically after adding 20% Si and then remains almost constant. The flame temperature decreases with increasing Si content, ranging from 2940 K to 2200 K and has the same trend as the computed adiabatic flame temperature (unlike the Ti case). The two systems show different behavior. The Al/Ti system shows no enhancement effects, i.e. the pure Ti case is most reactive on all counts with a smooth variation in combustion properties with varying fuel content. In contrast Si clears shows that mixing the two fuels can result in enhancement over each pure fuel.

3.3.2. T-Jump characterizations

Temperature-Jump wire ignition experiments were conducted to investigate the ignition behavior of the ternary systems. As shown in Fig. 4a, ignition temperature of Al/I_2O_5 drops significantly from ~ 850 K to ~ 610 K with 20% addition of Ti and asymptotically decreases to 570 K for Ti/I_2O_5. The Al/Si/I_2O_5 system shows a similar trend, although not dropping as precipitously.

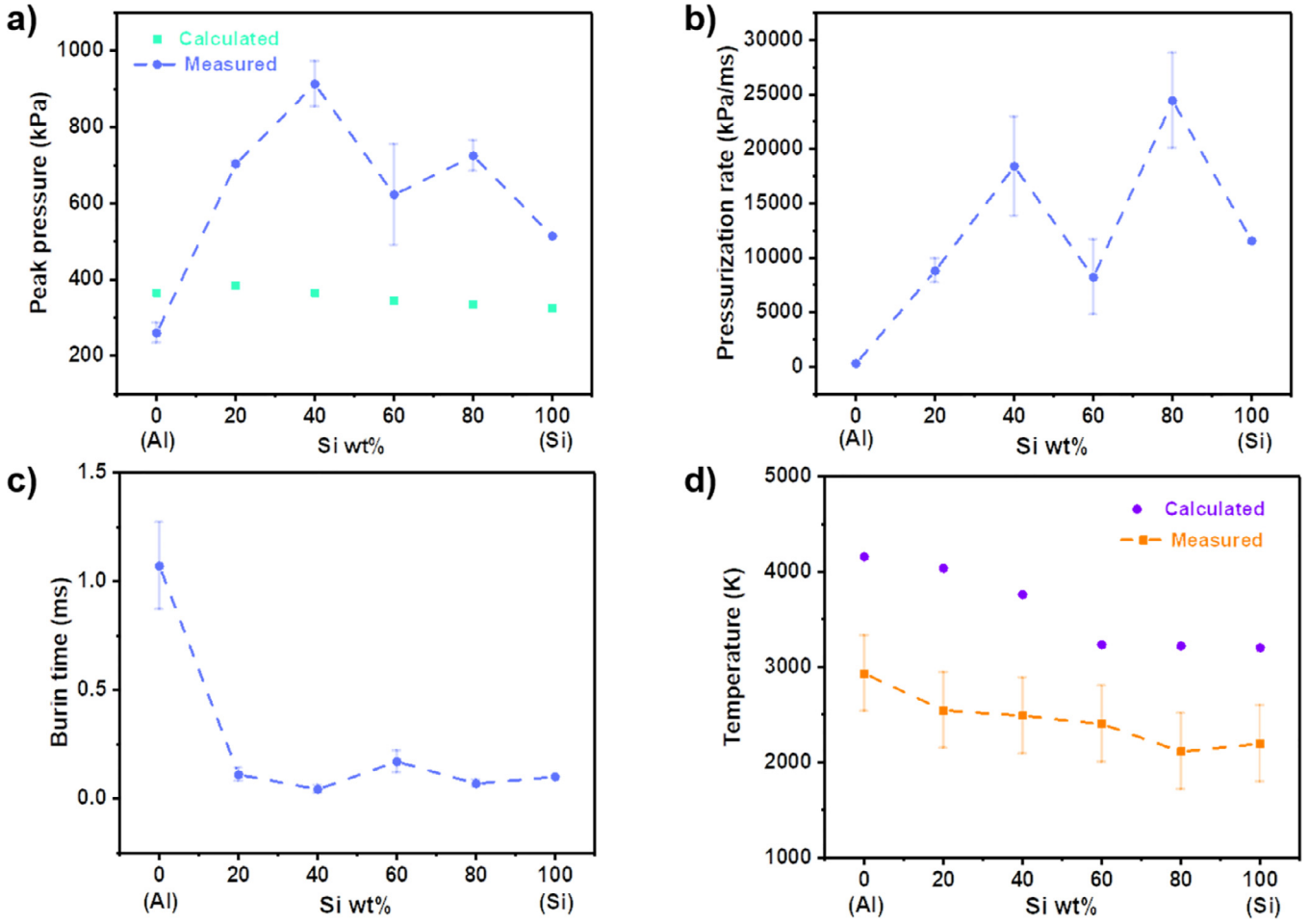

Fig. 3. Experimental and calculated peak pressure (a), pressurization rate (b) and burn time (c) of Al/Si/I_2O_5 system with different Si content in fuel. The reactivity is enhanced when Al and Si are combined as fuel. (d) Calculated adiabatic flame temperature and measured flame temperature in pressure cell. Experimental flame temperatures are lower than theoretical ones but the trend is similar. (For interpretation of the references to colour in this figure legend, the reader is referred to the web version of this article.)

Thus, in both cases additions of ~20% of either Ti or Si seem to have the most significant effect. The ignition events of these samples captured by high speed imaging are shown in Figure S3.

One interesting feature is the temperature (~ 690 K) for oxygen release from I_2O_5 (horizontal blue dotted line in Fig. 4a). Oxygen release temperature of I_2O_5 is lower than the ignition temperature of Al/I_2O_5 but higher than the rest of Al/Ti/I_2O_5 samples. For Al/Si/I_2O_5, 20% Si lowers the ignition temperature to the same as oxygen release temperature of neat I_2O_5. Above 20% Si, the ignition temperature is further lowered to below that critical temperature. This means that the addition of Ti and Si, even at relatively low content, shifts the initiation mechanism from gas phase dominated to condensed phase dominated [36–37]. This can significantly enhance the reactivity and energy release of the composite, because condensed phase reactions tend to have a shorter timescale and is less impaired by sintering, leading to faster reaction and higher reactivity [38]. It's worth noting that the oxygen release temperature of I_2O_5 in vacuum obtained from T-jump measurements is slightly higher than that (~630 K) in air [39]. The higher temperature is likely due to the high heating rate used in T-jump measurements that causes the temperature of the sample to lag behind the temperature of the wire. Therefore, it is reasonable to assume the decomposition behavior of I_2O_5 to be similar in vacuum and air.

Although the metal oxide shell is not reactive, it might affect the decomposition of the oxidizer. Previous work has reported that TiO_2 can catalyze the decomposition of $KClO_4$, evidenced by both lower oxygen release temperature and lower activation energy [18]. To explore this further, neat I_2O_5, a mixture of TiO_2 and I_2O_5, and a mixture of SiO_2 and I_2O_5 were characterized by thermogravimetric analysis. The results (Figure S4) show no significant difference in the decomposition behavior of these three samples, suggesting that TiO_2 and SiO_2 do not have a catalytic effect on I_2O_5.

Another important parameter for biocidal energetics is the release temperature of biocides, in this case, iodine. In order to investigate iodine release, Al/Ti/I_2O_5 and Al/Si/I_2O_5 samples were studied using the T-Jump TOFMS. The intensity of iodine signal (m/z = 127) versus temperature for Al/Ti/I_2O_5 and Al/Si/I_2O_5 samples is plotted in Fig. 4b and 4c, respectively. Iodine release profiles appear to be moving to lower temperatures but the widths of the profiles are relatively constant, implying that while one can use mixtures to tune the iodine release temperature, one really at least in these studies, changes the overall time scale for the release. The iodine release temperatures of the two systems are shown in Fig. 4d. After adding 20% of Ti or Si, the iodine release temperatures of both systems decrease significantly. Further addition of Ti or Si seems to have limited effect on iodine release temperature.

3.3.3. Energy release rate

Finally, we consider energy release rate, defined here as the amount of energy released normalize by the release time, us-

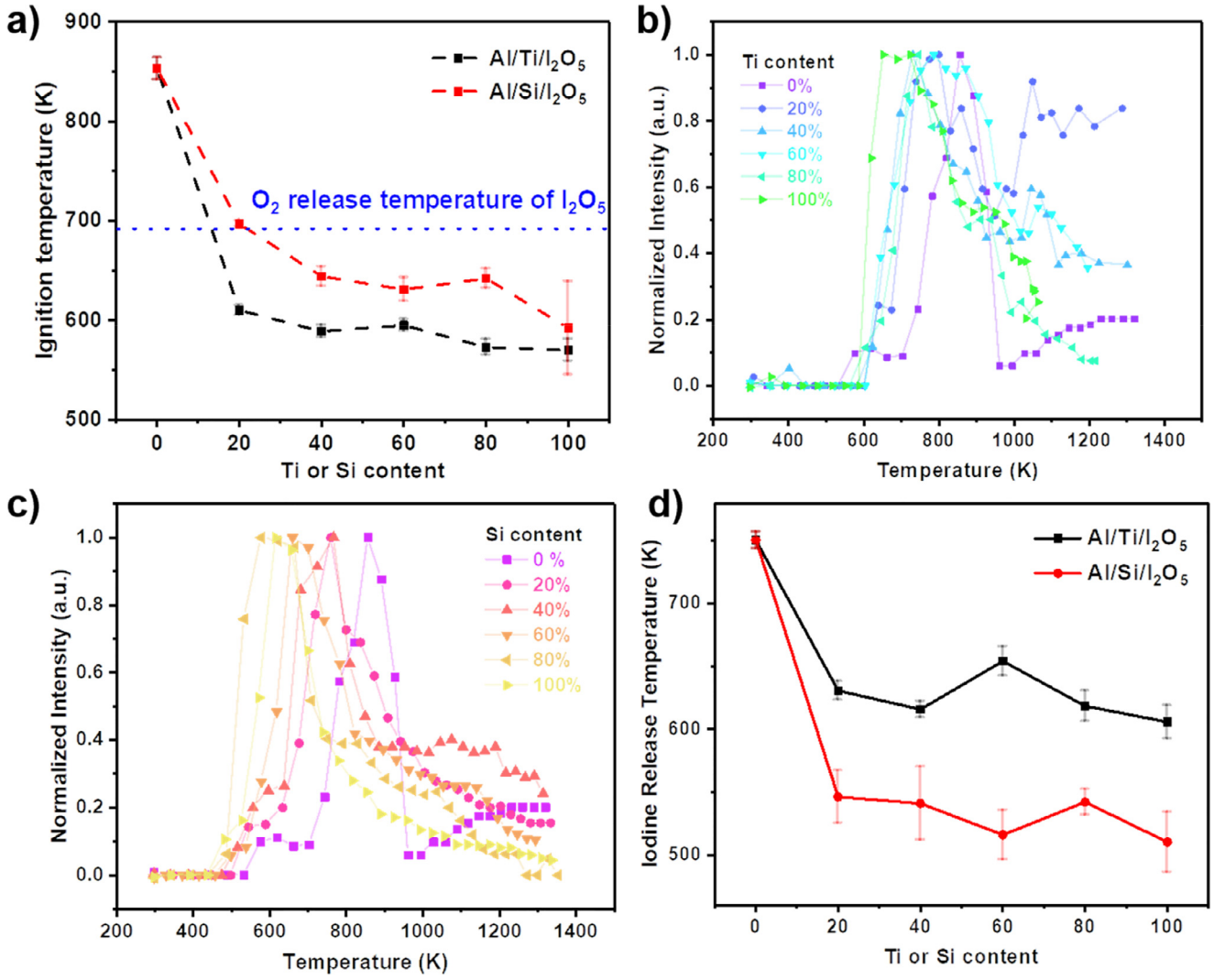

Fig. 4. (a) Ignition temperature of $Al/Ti/I_2O_5$ and $Al/Si/I_2O_5$ systems with different fuel compositions. The horizontal blue dotted line shows the oxygen release temperature of neat I_2O_5. (b) Iodine signal (m/z = 127) intensity of $Al/Ti/I_2O_5$ versus time. (c) Iodine signal (m/z = 127) of $Al/Si/I_2O_5$ versus time. (d) Onset temperature of iodine release for $Al/Ti/I_2O_5$ and $Al/Si/I_2O_5$ systems. (For interpretation of the references to colour in this figure legend, the reader is referred to the web version of this article.)

ing information extracted from the pressure cell results. Assuming that the heat generated by I_2O_5/metal reaction was absorbed by the combustion products and the heat loss is negligible given the rapidity of the reaction, the energy release rate can be expressed as:

$$R_E = \frac{\mathrm{m} \cdot \bar{c} \cdot (T_F - T_A)}{\Delta t}$$

In the above equation, m is the mass of the sample, which was kept constant for all samples. $\bar{c}$ is the specific heat capacity of each system. As previously mentioned, CHEETAH calculation was performed for constant volume condition and the active contents of fuels were considered. Based on the product species and their respective concentrations from CHEETAH calculation, the specific heat of the reaction products of each system was calculated as $\overline{c_v} = \sum c_i x_i$, where c_i is the specific heat of a product species and x_i is the mass fraction of the species. Four or five species with the highest concentrations were used for calculation. Condensed phase species were always used since they have a much larger specific heat than gaseous species. The calculation results are listed in Table S1. T_F is the flame temperature, T_A is the ambient temperature and Δt is the timescale of energy release which can be represented by the burn time.

The mass normalized energy release rate plotted versus burn time and flame temperature, are shown in Fig. 5a and 5b, respectively. The energy release rate is tuned over a wide range (20x). A clear correlation between R_E and burn time is shown in the plot, while the correlation of R_E with flame temperature is less evident. This result is expected considering the substantially more dramatic change in the burn time relative to the change in flame temperature, making the flame temperature a less decisive factor in tuning the energy release rate. The total energy release from CHEETAH calculation and experimental results for $Al/Ti/I_2O_5$ and $Al/Si/I_2O_5$ is also shown in Fig. 5c and 5d, respectively. The deviation of the experimental values from those predicted by CHEETAH code again suggests that the actual reaction is far from equilibrium state. The results suggest that Ti is a better fuel additive to Al in terms of preserving energy density. From a practical point of view, the energy release rate is manipulated through mainly change in timescale instead of energy, especially in the case of Ti, due to similar energetic performance of the selected fuels. This is desirable because the energy output is largely preserved while altering the timescale of the event.

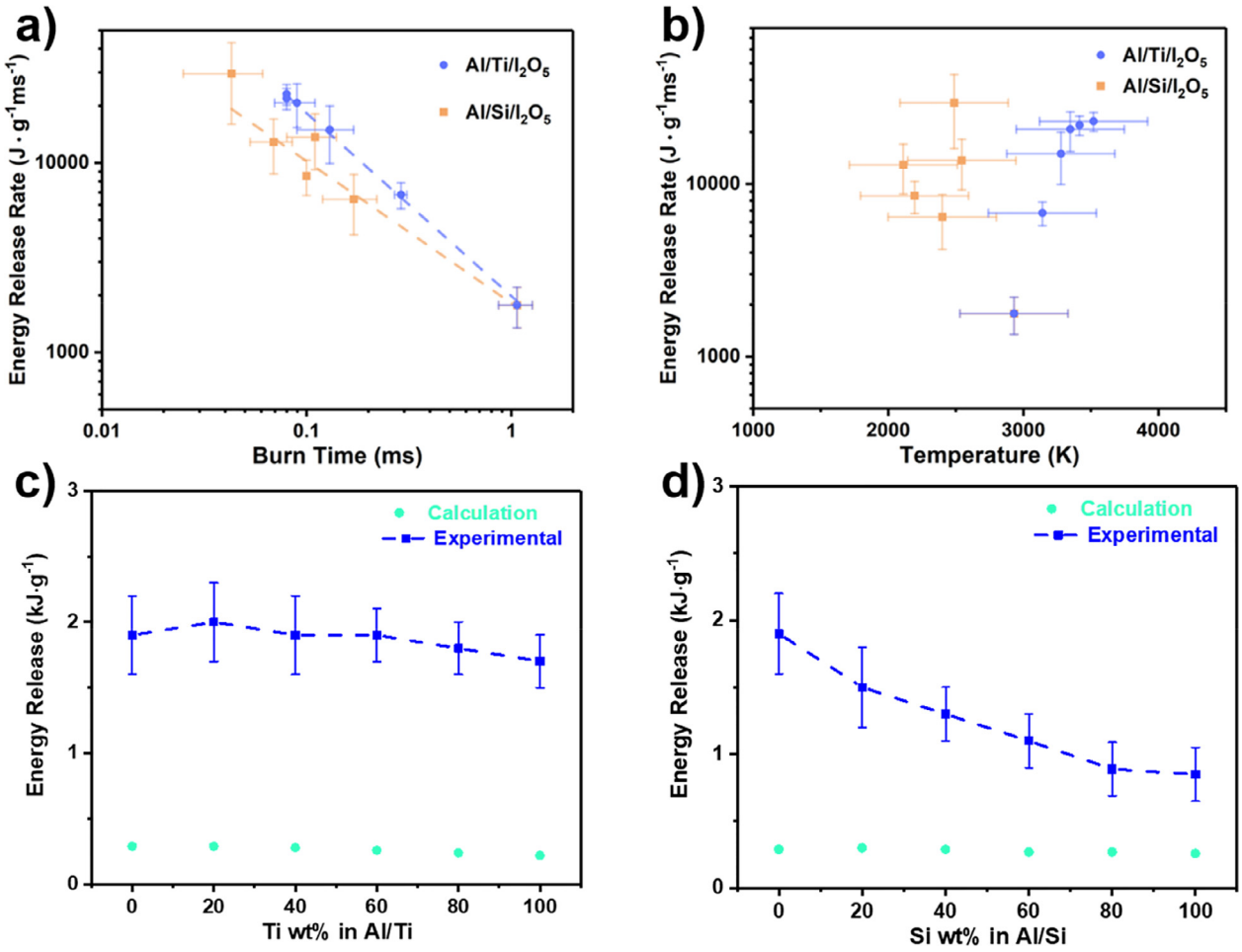

Fig. 5. Mass normalized energy release rate of Al/Ti/I_2O_5 and Al/Si/I_2O_5 versus burn time (a) and flame temperature (b). Calculated energy release using CHEETAH code and from experimental results for Al/Ti/I_2O_5 (c) and Al/Si/I_2O_5 (d).

4. Conclusion

I_2O_5 with various fuels and their mixtures were investigated. Single fuel studies with Al, Ti and Si suggested similar energy density but vastly different reactivity (Ti > Si ≫ Al). Based on the results, we conjectured that thermite mixtures with tunable reactivity and energy release rate could be formulated by combining different fuels. Therefore, Al/Ti/I_2O_5 and Al/Si/I_2O_5 systems with varying fuel compositions were studied.

Pressure cell measurements showed that the reactivity of the two systems varies with fuel composition. Al/Ti showed a simple mixing effect, i.e., higher reactivity at higher Ti content. While Al/Si showed an enhancing effect, namely the peak pressure and pressurization rate both increase first but peaks at 40% and 80%, respectively. Burn time is decreased drastically upon the addition of 20% Ti or Si. T-Jump characterizations showed that the addition of Ti or Si can shift the reaction pathway of Al/I_2O_5 from gas phase to condensed phase dominated initiation, resulting in a shorter reaction timescale. The change of the reaction mechanism is likely to be responsible for the enhanced reactivity.

Further discussion on the energy release rate concluded that the energy release rate can be tuned without considerably compromising energy output by using such ternary systems. The ability to alter reactivity and energy release rate while preserving high energy density makes this approach most promising for tailoring the properties of biocidal energetic systems.

Declaration of Competing Interest

The authors declare that they have no known competing financial interests or personal relationships that could have appeared to influence the work reported in this paper.

Acknowledgments

Support for this work comes from DTRA, the DTRA MSEE-URA and the AFOSR. L. Mangolini also acknowledges support from the National Science Foundation under award 1351386 (CAREER).

Supplementary materials

Supplementary material associated with this article can be found, in the online version, at doi:10.1016/j.combustflame.2020.12.047.

References

[1] B.R. Clark, M.L. Pantoya, The aluminium and iodine pentoxide reaction for the destruction of spore forming bacteria, Phys. Chem. Chem. Phys. 12 (2010) 12653–12657.
[2] O. Mulamba, E.M. Hunt, M.L. Pantoya, Neutralizing bacterial spores using halogenated energetic reactions, Biotechnol. Bioproc. E. 18 (2013) 918–925.
[3] W. Zhou, M.W. Orr, V.T. Lee, M.R. Zachariah, Synergistic effects of ultrafast heating and gaseous chlorine on the neutralization of bacterial spores, Chem. Eng. Sci. 144 (2016) 39–47.

[4] E.L. Dreizin, Metal-based reactive nanomaterials, Prog. Energy Combust. Sci. 35 (2009) 141–167.
[5] B. Khasainov, M. Comet, B. Veyssiere, D. Spitzer, Comparison of performance of fast-reacting nanothermites and primary explosives, Propellants Explos. Pyrotech. 42 (2017) 754–772.
[6] T. Wu, M.R. Zachariah, Silver ferrite: a superior oxidizer for thermite-driven biocidal nanoenergetic materials, RSC Adv 9 (2019) 1831–1840.
[7] K.T. Sullivan, C. Wu, N.W. Piekiel, K. Gaskell, M.R. Zachariah, Synthesis and reactivity of nano-Ag2O as an oxidizer for energetic systems yielding antimicrobial products, Combust. Flame 160 (2013) 438–446.
[8] W. Zhou, J.B. DeLisio, X. Li, L. Liu, M.R. Zachariah, Persulfate salt as an oxidizer for biocidal energetic nano-thermites, J. Mater. Chem. A 3 (2015) 11838–11846.
[9] H. Wang, G. Jian, W. Zhou, J.B. DeLisio, V.T. Lee, M.R. Zachariah, Metal iodate-based energetic composites and their combustion and biocidal performance, ACS Appl. Mater. Interfaces 7 (2015) 17363–17370.
[10] J. Feng, G. Jian, Q. Liu, M.R. Zachariah, Passivated iodine pentoxide oxidizer for potential biocidal nanoenergetic applications, ACS Appl. Mater. Interfaces 5 (2013) 8875–8880.
[11] T. Wu, X. Wang, P.Y. Zavalij, J.B. DeLisio, H. Wang, M.R. Zachariah, Performance of iodine oxides/iodic acids as oxidizers in thermite systems, Combust. Flame 191 (2018) 335–342.
[12] K.S. Martirosyan, L. Wang, D. Luss, Novel nanoenergetic system based on iodine pentoxide, Chem. Phys. Lett. 483 (2009) 107–110.
[13] A. Prakash, A.V. McCormick, M.R. Zachariah, Tuning the reactivity of energetic nanoparticles by creation of a core−shell nanostructure, Nano Lett 5 (2005) 1357–1360.
[14] G.M. Dutro, R.A. Yetter, G.A. Risha, S.F. Son, The effect of stoichiometry on the combustion behavior of a nanoscale Al/MoO_3 thermite, Proc. Combust. Inst. 32 (2009) 1921–1928.
[15] J.A. Puszynski, C.J. Bulian, J.J. Swiatkiewicz, Processing and ignition characteristics of aluminum-bismuth trioxide nanothermite system, J. Propul. Power 23 (2007) 698–706.
[16] J. Dai, F. Wang, C. Ru, J. Xu, C. Wang, W. Zhang, Y. Ye, R. Shen, Ammonium perchlorate as an effective additive for enhancing the combustion and propulsion performance of Al/CuO nanothermites, J. Phys. Chem. C 122 (2018) 10240–10247.
[17] M. Comet, C. Martin, F. Schnell, D. Spitzer, Nanothermites: a short review. Factsheet for experimenters, present and future challenges, Propellants Explos. Pyrotech. 44 (2019) 18–36.
[18] M.C. Rehwoldt, Y. Yang, H. Wang, S. Holdren, M.R. Zachariah, Ignition of nanoscale titanium/potassium perchlorate pyrotechnic powder: reaction mechanism study, J. Phys. Chem. C 122 (2018) 10792–10800.
[19] R. Thiruvengadathan, G.M. Belarde, A. Bezmelnitsyn, M. Shub, W. Balas-Hummers, K. Gangopadhyay, S. Gangopadhyay, Combustion characteristics of silicon-based nanoenergetic formulations with reduced electrostatic discharge sensitivity, Propellants Explos. Pyrotech. 37 (2012) 359–372.
[20] L. Mangolini, E. Thimsen, U. Kortshagen, High-yield plasma synthesis of luminescent silicon nanocrystals, Nano Lett 5 (2005) 655–659.
[21] A. Woodard, K. Shojaei, G. Nava, L. Mangolini, Graphitization of carbon particles in a non-thermal plasma reactor, plasma chem, Plasma P 38 (2018) 683–694.
[22] A. Alvarez Barragan, N.V. Ilawe, L. Zhong, B.M. Wong, L. Mangolini, A non-thermal plasma route to plasmonic TiN nanoparticles, J. Phys. Chem. C 121 (2017) 2316–2322.
[23] S. Exarhos, A. Alvarez-Barragan, E. Aytan, A.A. Balandin, L. Mangolini, Plasmonic core–shell zirconium nitride–silicon oxynitride nanoparticles, ACS Energy Lett 3 (2018) 2349–2356.
[24] U.R. Kortshagen, R.M. Sankaran, R.N. Pereira, S.L. Girshick, J.J. Wu, E.S. Aydil, Nonthermal plasma synthesis of nanocrystals: fundamental principles, materials, and applications, Chem. Rev 116 (2016) 11061–11127.
[25] T. Lopez, L. Mangolini, Low activation energy for the crystallization of amorphous silicon nanoparticles, Nanoscale 6 (2014) 1286–1294.
[26] A. Alvarez Barragan, G. Nava, N.J. Wagner, L. Mangolini, Silicon-carbon composites for lithium-ion batteries: a comparative study of different carbon deposition approaches, J. Vac. Sci. Technol. B 36 (2018) 011402.
[27] G. Nava, F. Fumagalli, S. Gambino, I. Farella, G. Dell'Erba, D. Beretta, G. Divitini, C. Ducati, M. Caironi, A. Cola, F. Di Fonzo, Towards an electronic grade nanoparticle-assembled silicon thin film by ballistic deposition at room temperature: the deposition method, and structural and electronic properties, J. Mater. Chem. C 5 (2017) 3725–3735.
[28] R.J. Jacob, D.J. Kline, M.R. Zachariah, High speed 2-dimensional temperature measurements of nanothermite composites: probing thermal vs gas generation effects, J. Appl. Phys. 123 (2018) 115902.
[29] L. Zhou, N. Piekiel, S. Chowdhury, M.R. Zachariah, T-Jump/time-of-flight mass spectrometry for time-resolved analysis of energetic materials, Rapid Commun. Mass. Spectrom. 23 (2009) 194–202.
[30] L. Zhou, N. Piekiel, S. Chowdhury, M.R. Zachariah, Time-resolved mass spectrometry of the exothermic reaction between nanoaluminum and metal oxides: the role of oxygen release, J. Phys. Chem. C 114 (2010) 14269–14275.
[31] B.K. Little, S.B. Emery, J.C. Nittinger, R.C. Fantasia, C.M. Lindsay, Physiochemical Characterization of Iodine(V) Oxide, Part 1: hydration Rates, Propellants Explos. Pyrotech. 40 (2015) 595–603.
[32] D.K. Smith, K. Hill, M.L. Pantoya, J.S. Parkey, M. Kesmez, Reactive characterization of anhydrous iodine (v) oxide (I2O5) with aluminum: amorphous versus crystalline microstructures, Thermochim. Acta 641 (2016) 55–62.
[33] D.K. Smith, J. McCollum, M.L. Pantoya, Effect of environment on iodine oxidation state and reactivity with aluminum, Phys. Chem. Chem. Phys. 18 (2016) 11243–11250.
[34] T. Wu, A. SyBing, X. Wang, M.R. Zachariah, Aerosol synthesis of phase pure iodine/iodic biocide microparticles, J. Mater. Res. 32 (2017) 890–896.
[35] R.J. Jacob, D.L. Ortiz-Montalvo, K.R. Overdeep, T.P. Weihs, M.R. Zachariah, Incomplete reactions in nanothermite composites, J. Appl. Phys. 121 (2017) 054307.
[36] G. Jian, S. Chowdhury, K. Sullivan, M.R. Zachariah, Nanothermite reactions: is gas phase oxygen generation from the oxygen carrier an essential prerequisite to ignition? Combust. Flame 160 (2013) 432–437.
[37] N.W. Piekiel, L. Zhou, K.T. Sullivan, S. Chowdhury, G.C. Egan, M.R. Zachariah, Initiation and Reaction in Al/Bi_2O_3nanothermites: evidence for the predominance of condensed phase chemistry, Combust. Sci. Technol. 186 (2014) 1209–1224.
[38] R.J. Jacob, G. Jian, P.M. Guerieri, M.R. Zachariah, Energy release pathways in nanothermites follow through the condensed state, Combust. Flame 162 (2015) 258–264.
[39] B.K. Little, S.B. Emery, J.C. Nittinger, R.C. Fantasia, C.M. Lindsay, Physiochemical Characterization of iodine(V) oxide, part 1: hydration rates, Propellants Explos. Pyrotech. 40 (2015) 595–603.